energies

MDPI

Article

Applied Machine Learning to Study the Movement of Air Masses in the Wind Farm Area

Vladislav N. Kovalnogov *, Ruslan V. Fedorov, Andrei V. Chukalin *, Vladimir N. Klyachkin, Vladimir P. Tabakov and Denis A. Demidov

Laboratory of Interdisciplinary Problems in Energy Production, Ulyanovsk State Technical University, 32 Severny Venetz Street, 432027 Ulyanovsk, Russia; r.fedorov@ulstu.ru (R.V.F.); v_kl@mail.ru (V.N.K.); vpt@ulstu.ru (V.P.T.); d.demidov@ulstu.ru (D.A.D.)

* Correspondence: kvn@ulstu.ru (V.N.K.); chukalin.andrej@mail.ru (A.V.C.)

Abstract: Modeling the atmospheric boundary layer (ABL) in the area of a wind farm using computational fluid dynamics (CFD) methods allows us to study the characteristics of air movement, the shading effect, the influence of relief, etc., and can be actively used in studies of local territories where powerful wind farms are planned to be located. The operating modes of a wind farm largely depend on meteorological phenomena, the intensity and duration of which cause suboptimal operating modes of wind farms, which require the use of modern tools for forecasting and classifying precipitation. The methods and approaches used to predict meteorological phenomena are well known. However, for designed and operated wind farms, the influence of meteorological phenomena on the operating modes, such as freezing rain and hail, remains an urgent problem. This study presents a multi-layered neural network for the classification of precipitation zones, designed to identify adverse meteorological phenomena for wind farms according to weather stations. The neural network receives ten inputs and has direct signal propagation between six hidden layers. During the training of the neural network, an overall accuracy of 81.78%, macro-average memorization of 81.07%, and macro-average memorization of 75.05% were achieved. The neural network is part of an analytical module for making decisions on the application of control actions (control of the boundary layer of the atmosphere by injection of silver iodide, ionization, etc.) and the formation of the initial conditions for CFD modeling. Using the example of the Ulyanovsk wind farm, a study on the movement of air masses in the area of the wind farm was conducted using the initial conditions of the neural network. Digital models of wind turbines and terrain were created in the Simcenter STAR-CCM+ software package, version 2022.1; an approach based on a LES model using an actuating drive disk model (ADM) was implemented for modeling, allowing calculation with an error not exceeding 5%. According to the results of the modeling of the current layout of the wind turbines of the Ulyanovsk wind farm, a significant overlap of the turbulent wake of the wind turbines and an increase in the speed deficit in the area of the wind farm were noted, which significantly reduced its efficiency. A shortage of speed in the near and far tracks was determined for special cases of group placement of wind turbines.

Keywords: wind farm; mathematical modeling; computational fluid dynamics; atmospheric boundary layer; neural network; machine learning; actuator disk model; weather station

Citation: Kovalnogov, V.N.; Fedorov, R.V.; Chukalin, A.V.; Klyachkin, V.N.; Tabakov, V.P.; Demidov, D.A. Applied Machine Learning to Study the Movement of Air Masses in the Wind Farm Area. *Energies* **2024**, *17*, 3961. https://doi.org/10.3390/en17163961

Academic Editor: Young-Min Wi

Received: 11 July 2024
Revised: 31 July 2024
Accepted: 7 August 2024
Published: 9 August 2024

1. Introduction

The active development of wind energy makes it possible to introduce large capacities into energy systems, but it requires solving many problems associated with the high uncertainty of wind energy potential and meteorological phenomena [1].

The Russian Federation, which possesses large areas and regions with high wind potential, has the opportunity to set up heavy-duty wind farms. Forecasting wind potential by considering meteorological phenomena and modeling the air movement in the area of a

wind farm makes it possible to create optimized wind farms considering the characteristics of regions at the design stage, obtaining accurate forecasts of electricity generation, and exploring the possibilities of influencing meteorological phenomena [2].

Various methods have been developed to predict wind characteristics, which can be classified according to time scales. In turn, forecasting wind characteristics based on their temporal nature can be divided into several categories: forecasting eight hours ahead (short-term forecasting), day-ahead forecasting (medium-term forecasting), and forecasting several days in advance (long-term forecasting). It is also worth noting that schemes for predicting wind characteristics can be classified according to methodological features: a physical method based on the state of the lower atmosphere or numerical weather forecast using archival data; statistical method using artificial intelligence tools (for example, neural networks) and time series analysis approaches for processing "Big Data" (Big Data); a hybrid method that combines physical and statistical methods [3].

For wind farms to operate effectively, weather forecasting must involve extensive research using advanced deep learning techniques. For example, in [4] a fully connected convolutional LSTM network was proposed to predict short-term future precipitation intensity in a local area and extract the spatiotemporal dynamics of the data. Similar to the work in [5], a predictive model for temperature and wind speed from 1 to 10 days in advance using a convolutional neural network was proposed. The 1D-CNN-based architecture processes 3D tensor data and extracts spatiotemporal relationships. In [6], a weather forecasting model using LSTM and temporal convolutional networks was presented. According to the authors, the results obtained were more accurate than those of classical time-series forecasting [7].

Application systems for forecasting wind potential, as well as the power generated by a wind farm, include hybrid modeling systems, an example of which is WindSim software, version 11. Hybrid modeling includes Numerical Weather Prediction (NWP), Artificial Neural Network (ANN), and Computational Fluid Dynamics (CFD), combining physical and statistical methods. Several institutes and organizations have devoted extensive research to improving methods for predicting wind characteristics. Models such as WPMS, WPPT, Prediktor, ARMINES, and Previento have been developed and implemented in wind farms around the world. These models are based on physical, static, and hybrid methods. In [8], internationally developed wind power forecasting software models were presented.

It should be noted that meteorological phenomena, their intensity and duration, cause unsteady operating modes of wind power plants, which requires the development of solutions for safe and reliable operation [9]. The region under consideration is characterized by frequent temperature transitions beyond 0 °C, which can lead to icing of wind turbine blades. Owing to the ability of machine learning systems, it is possible to predict the control impacts and precipitation management on the ABL. Rainfall management can be implemented in several ways [10], but the most studied method is seeding clouds with moisture concentrators. Currently, such influences are mainly based on a change in the phase state of the cloud when it is "seeded" with certain reagents, in particular, solid carbon dioxide and silver iodide smoke. When crushed carbon dioxide evaporates in supercooled water clouds, strong cooling (below −40 °C) and supersaturation are created, which leads to crystallization. The clouds turn into mixed clouds; as a result, they acquire colloidal instability and produce precipitation, as occurs naturally in mixed clouds. Silver iodide smoke aerosols also cause supercooled droplets to freeze, acting as freeze or sublimation nuclei. The appearance of a solid phase in powerful cumulus clouds, as well as the enlargement of droplets, can be caused by the injection of sprayed water into the clouds, the droplets of which grow owing to coagulation. Hygroscopic particles or droplets (of salt solutions) introduced into clouds can cause precipitation without a solid phase falling out of the cloud. Microscopic particles of silver iodide were captured by supercooled droplets, turning into crystals that became artificial hail nuclei. The latter enters into competition with natural hail embryos for the moisture contained in the cloud and does not allow hailstones to grow to large sizes. As a result, a huge number of small hailstones form in

the cloud, which, when falling from the cloud, have time to melt in the warm part of the atmosphere and reach the ground in the form of rain. Reagents are introduced into clouds by seeding the cloud with granular solid carbon dioxide from an airplane or drone or by creating fumes of silver iodide in special generators.

Modeling the ABL using CFD packages makes it possible to predict the structure of the ABL accurately in the area where the wind farm is located. In this case, it is extremely important to adequately describe the processes occurring in the ABL depending on the stability of the atmosphere. Therefore, a prerequisite is the correct setting of the boundary weather conditions (velocity profiles, temperatures, turbulent characteristics, etc.). The evolution of the ABL is determined directly by the influence of the underlying surface and turbulence, which is well developed in the area where the wind farm is located. This can be seen most clearly in the vertical distribution of wind speed. The nature of the vertical distribution of wind speed between the underlying surface and the upper boundary of the atmospheric boundary layer is determined by turbulence, which causes an exchange of momentum between different layers. Turbulence not only affects the distribution of meteorological quantities at an altitude, but also depends on gradients. The fields of meteorological quantities and turbulent exchange change interconnectedly under the influence of external factors. These include the influx of solar radiation and the horizontal pressure gradient, and the intensity of heat and mass transfer between the boundary layer, the free atmosphere, and the upper layers of the soil. A change in any external factor subsequently leads to a change in the profile of meteorological quantities. For example, if the influx of solar radiation to the Earth increases, the temperature of the underlying surface increases [11]. In addition, in the territory of wind farms, the appearance and movement of liquid and solid particles is possible, which, under certain conditions, can have a significant impact on turbulent exchange. When mathematically modeling flows with a dispersed phase, it is important to correctly set up the initial conditions, adequately specifying the main parameters that determine the system. The carrier medium can be a liquid or gas, and the dispersed phase can be solid particles, liquid droplets, or gas bubbles [12]. Various particles carried by air in the ABL can cause build-up and damage to wind turbine blades.

There is a steady trend in the use of powerful computing systems to solve multiscale problems in relation to wind farms. This trend is formed on the basis of the availability of computing power, as well as the emergence of new approaches to modeling, which allows us to adequately describe real systems with high accuracy [13–16]. There are three approaches to the mathematical modeling of the movement of air masses in the field of wind turbines on the scale of the atmospheric boundary layer. The first approach is based on the use of Reynolds-averaged Navier–Stokes (RANS) equations. The second approach is Large eddy simulation (LES). The third approach is direct numerical modeling (DNS), which requires the largest amount of computational resources from the presented methods. It should be noted at once that the use of the first approach in most early studies of ABL was highly widespread [17–21]. This approach makes it possible to calculate the average values of the flow parameters, taking into account the vortex flow using turbulence models. One-dimensional, two-dimensional, and three-dimensional models are used. A one-dimensional model is used in the form of blocks characterizing geophysical turbulence on a large scale ABL [22,23].

The RANS approach has limitations related to the prediction of complex flows with instability or significant separation. When studying wind farms on an ABL scale, a more reliable approach is LES [24,25]. The peculiarity of the LES model is the description of statistical characteristics of large-scale turbulent eddies taking into account molecular viscosity and small-scale turbulent flow pulsation. The use of this approach allows obtaining reliable results for the study of wind turbine wakes at ABL scales under non-stationary conditions, which will allow for effective prediction of the generated power. However, the quality of calculations directly depends on the grid scale. The LES model, in comparison

with RANS, is more demanding on the quality of the grid, which increases the calculation time [26,27].

To describe air flows in the area of wind turbine blades in a wide spatial and temporal interval, the "high fidelity modeling" (HFM) approach is used. Three categories of HFM should be distinguished for wind turbine modeling: blade resolution models (BRM), actuator linear models (ALM), and actuator disc models (ADM) [28,29]. The use of approaches based on the virtual disk model allows one to reduce the calculation time by simulating the operation of the blades, while maintaining the accuracy of reproduction of the wake behind the wind turbine. The use of the LES model together with the virtual disk makes it possible to study the wind farm, spending moderate computing resources, in connection with which many authors have recently been actively using these approaches in their works. However, this approach will not allow one to study the flows in the boundary layer region at the ends of the blades, where complex vortex structures of the flow are observed, which causes a significant decrease in the kinetic energy of the wind behind the wind turbine. A description of this phenomenon is presented in the works [30–32].

There are a number of simplified hypotheses, such as Taylor's frozen turbulence hypothesis and Kolmogorov's idea of cascade energy transfer, which have been used to study wind turbine wakes. In his work, Strizhak S. [33] considered a single wind turbine using the LES approach and the ALM disk model. The results showed good convergence of the solution, due to the use of the Smagorinsky model, which allows calculation of the values of turbulent subgrid viscosity

The development of intelligent systems due to the availability of computing resources and significant scientific advances has become widespread in recent decades. The ability to work with large amounts of data allows the use of intelligent systems to analyze research results. The use of a neural network for processing the results of a numerical study is discussed in [34]. Using this approach, it was possible to generalize models for predicting the turbulent wake of wind turbines. This will make it possible to study in detail the dependence of wind speed and yaw angles on electricity generation by wind turbines. An adequate wind farm model depends on a number of initial and boundary conditions. When preparing data, it is necessary to take into account surface orography, stratification, convection, solar radiation, and many other factors [18]. A separate challenge in data preparation is the multiscale nature of the ABL, for which flow can be limited to 1000 m above the surface of the wind farm. This condition is applicable for small wind farms located on flat terrain. When considering wind farms located over tens of square kilometers, the affected boundary layer height can be significantly higher. When considering limited areas (near wake and far wake of wind turbines), the problem of multiscale disappears. The scale of the computing areas of wind farms requires significant computational costs and software for calculations. The analysis of the literature showed that most of the research is carried out in the ANSYS Fluent, SFX and STAR CCM+ programs. Researchers have also proposed their own non-commercial products, examples of which are [35–38].

The influence of terrain orography on the formation of ABL is considered in the works [39–41]. In their works, the authors note the significant influence of relief on the dynamics of air flow and the formation of the underlying surface in the area of wind turbines. To achieve high computational accuracy using LES models in ABL simulations with distributed surface wind turbines, it is necessary to parameterize the turbulent flows at the subgrid scale (SGS).

The third method is based on the numerical solution of Navier–Stokes differential equations. This method requires a high spatiotemporal resolution and, therefore, requires considerable computing power. Therefore, it is rarely used to obtain large datasets of turbulent flows with simple structures. The LES method is the optimal approach for modeling because of the trade-off between computer time consumption and calculation accuracy. To optimize the calculation processes, this study proposes an approach based on the use of the ADM model [42–44] of a Vestas V126-3.45 MW wind turbine using the one-dimensional impulse method (1D-Momentum), including data on the power curve and

simulated wind turbine force coefficients. A tangible advantage of ADM is the simulation of a wind turbine rotor, which greatly simplifies the preparation of the model and structure of the computational grid used. This paper presents the results of modeling the movement of air masses in the area of wind turbines on the scale of the surface boundary layer of the atmosphere for an aligned and staggered layout of wind turbines.

Based on the analysis of literature sources, it can be noted that hybrid modeling is an advanced approach to the design of wind farms. An urgent direction in the development of these approaches is the possibility of assessing meteorological phenomena that can lead to the disruption of wind farms as well as detailed CFD modeling. This study presents a neural network for classifying precipitation zones based on data from weather stations, which allows the identification of adverse meteorological phenomena (icy rain, hail) with high accuracy, Section 2. The neural network is part of an analytical module for making decisions on the application of control actions (control of the atmospheric boundary layer by injection of silver iodide, ionization, etc.) and the formation of initial conditions for CFD modeling. Using the example of the Ulyanovsk Wind Farm, an approach to CFD modeling is proposed to study the movement of air masses based on the LES model using the actuator model of the drive disk (ADM), Section 3. The layout of the wind turbines of the Ulyanovsk wind farm was presented in [45]. Section 4 presents the results of a numerical study of the atmospheric boundary layer in the area of the wind farm in the speed range from 6 to 12 m/s, a speed deficit in the near and far wake is determined for special cases of group placement of wind turbines. Based on the results of the work, conclusions are formulated and the main research results are presented, Section 5.

2. Materials and Methods

2.1. Neural Network

The main goal of using machine learning methods to predict and classify precipitation in selected areas with a radius of up to 500 km is to achieve more accurate and reliable results. These methods, particularly the hybridization of numerical weather prediction (NWP) and machine learning (ML), including artificial neural networks (ANNs), are modern tools that scientists and researchers are increasingly using in their work, thereby increasing the accuracy of their forecasts [46].

NWP methods are based on mathematical models of the atmosphere and other physical processes that affect the weather conditions. However, even the most accurate models still have limitations and some degree of uncertainty when forecasting over the long term and relatively small areas. In this case, machine learning methods can be useful for refining and improving forecasts.

ANNs mimic the function of the human brain and are capable of processing and analyzing large amounts of data and extracting patterns from it. Training neural networks using historical precipitation data allows the creation of models that can predict future weather conditions with high accuracy.

Training ANNs on historical precipitation data allows for the creation of models that can predict future weather conditions with high accuracy. Another important feature of these methods is their adaptability and ability to increase the accuracy of forecasts with the accumulation of new data and model updates.

An ANN is a general-purpose approximator for nonlinear functions that consists of an input layer, one or more hidden layers, and an output layer that contains predicted values. Each layer comprises neurons that process information before passing it to the next layer. Connections between neurons have a weight that characterizes the level of connectivity of information passing through these neurons in different layers of the network. The operating principle and mathematical definition of an individual neuron in such a network are shown in Figure 1. A neural network with feedforward signal propagation, consisting of one or many hidden layers, is called a multilayer perceptron.

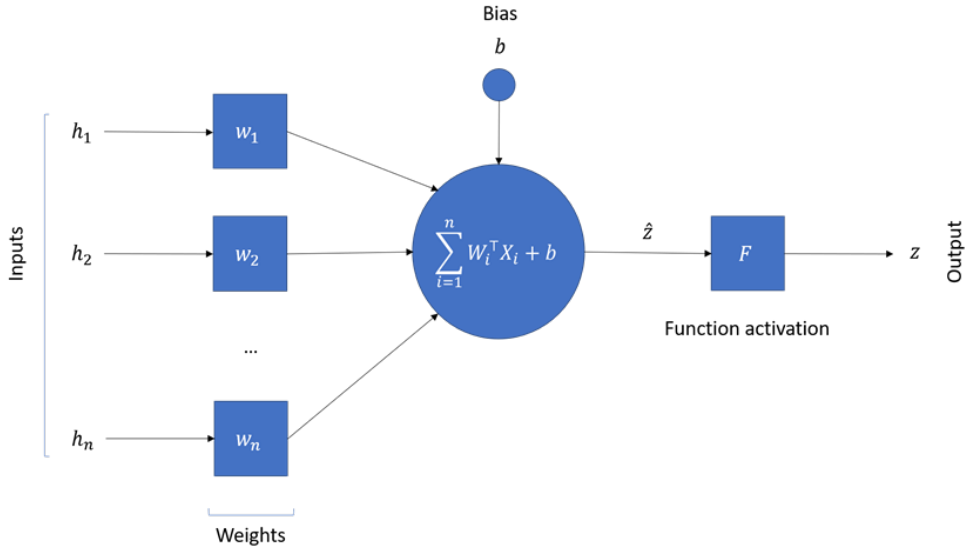

Figure 1. A fundamental example of how a single neuron works in a network.

A function activation is used to determine the output value of a neuron based on the weighted sum of the input values and the bias. The presence of a function activation allows the network to find more complex dependencies and solve problems with nonlinear dependencies in the data. It determines whether information from the neuron will be transmitted further through the network or its distribution will be interrupted. The function activation takes the result of a weighted sum as input and converts it into a specific output signal. It determines whether the information received from a given neuron will be transmitted further along the network or its distribution will be interrupted. The choice of the function activation depends on the characteristics of the problem and the requirements for the model. The optimal choice allows the network to effectively model complex dependencies and achieve high results in solving machine learning problems. The most common functions activation are as follows:

1. Sigmoid—this converts input values ranging from 0 to 1 or from −1 to 1 respectively;
2. Tanh—this takes values in the range [−1; 1];
3. The Rectified Linear Unit (ReLU)—this accepts values from zero to the maximum positive value passed to the function.
4. Leaky ReLU—this is a modification of ReLU that allows you to return a small value if the argument is negative;
5. Softmax—this converts input values into probabilistic values and is used when it is necessary to divide data into several classes.

The indicators of accuracy, completeness, and accuracy were used to assess the accuracy of the resulting model. These indicators were used to assess the quality of classification models. Precision is the proportion of observations that belong to a given class relative to all observations assigned by the system to that class. Completeness is the proportion of observations found by the classifier belonging to a class relative to all the observations of this class in the test sample. Accuracy shows the total number of correctly classified observations relative to all observations in the sample. The purpose of training the system is to accurately predict and classify the probability of precipitation in a given area, considering control actions.

2.2. The Network Architecture

The developed neural network takes 10 parameters of weather conditions at the input layer, after which the signal passes through 6 hidden layers, where each layer contains 60 neurons. Each layer uses a function activation *relu*:

$$relu(\hat{z}) = max(0, \hat{z}) \quad (1)$$

where $\hat{z}$ is a output value of the neuron.

For the output layer, a multi-variable logistic function is used as the function activation σ ($softmax$):

$$\sigma(z)_i = \frac{e^{z_i}}{\sum_{k=1}^{K} e^{z_k}} \quad (2)$$

where z is a vector of values obtained from the linear layer of the neural network; e is a exponent function; i, k are the vector values z.

A detailed description of the presented activation functions is presented in the work [47].

The architecture of the developed neural network is shown in Figure 2.

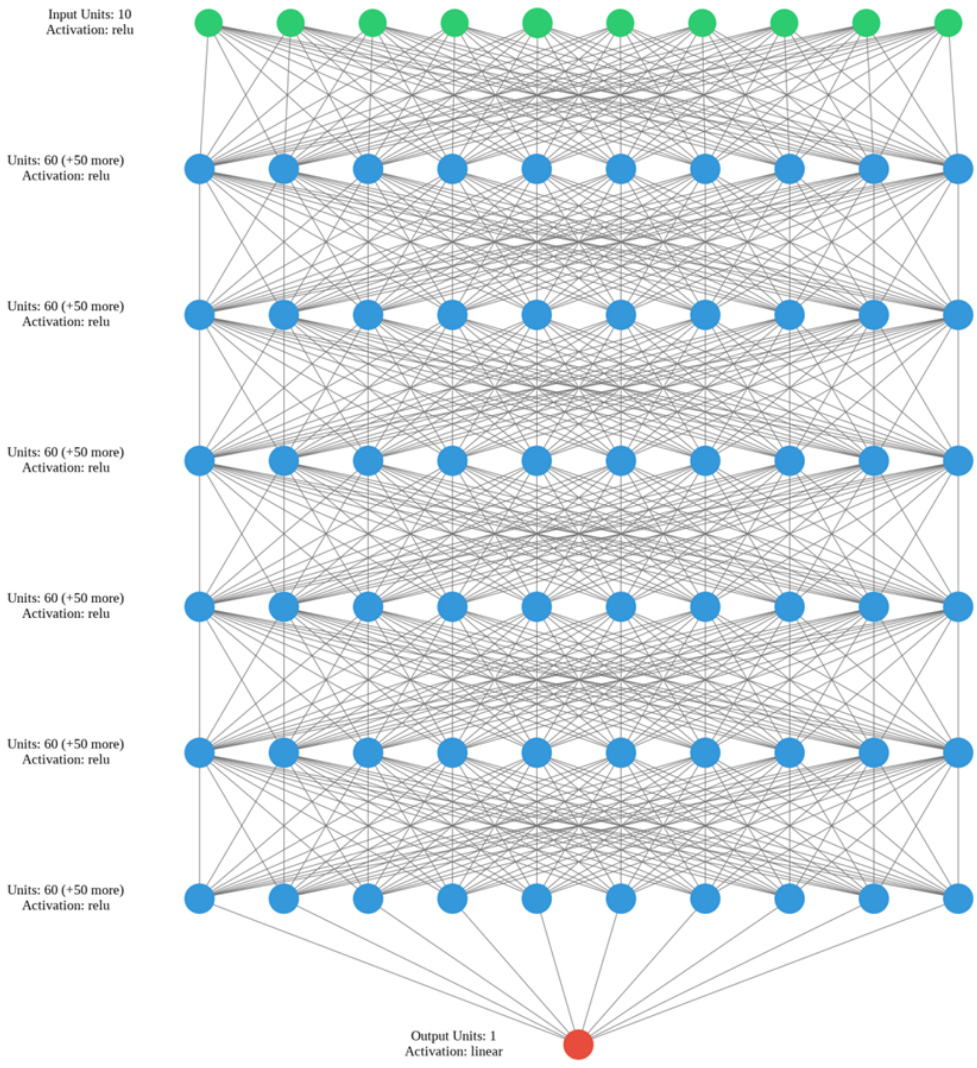

Figure 2. The network architecture.

The following weather characteristics were used as input data:
Wind speed, m/s;
Wind direction, values in degrees;
Direction of the weather station relative to the wind farm, values in degrees;
Distance to weather station, m;
Air temperature, °C;
Dew point temperature, °C;

Relative humidity, %;
Atmospheric pressure, hPa;
Precipitation amount, mm;
Cloud height, m.

The output shows the probability of formation of the following types of precipitation or their absence: weather phenomena (weather characteristics), rain, snow, hail, blizzard, fog, clear weather.

The above data coming from the external environment were converted and coded for application. The coding of the code for each parameter was carried out based on the conditions of estimated significance for input data and the probabilistic phenomenon for output data. Coded values ranged from 0.01 to 0.99 from minimum to maximum values. Four classes were obtained based on the presented data: 0—no precipitation; 1—crystalline precipitation; 2—precipitation in liquid form; 3—fog, drizzle. These classes were identified based on the presence of values other than 0 for the indicator of the total precipitation per day. It is worth noting that the use of this classifier outputs not four discrete values, 0 or 1, but continuous values in the range (0, 1), which corresponds to the probability that the class of precipitation predominates according to the given meteorological data.

2.3. Weather Stations

The ability to classify, forecast, and manage meteorological phenomena makes it possible to manage risks during the design and operation of wind farms. Machine learning systems have been widely applied because the developed models and approaches [48] enable the description of changes in the states of a controlled system based on learning.

It is necessary to prepare training data to solve a given problem using neural networks. The analysis of the region enabled the identification of eight meteorological stations around the wind farm containing archival weather data (see Figure 3) [49].

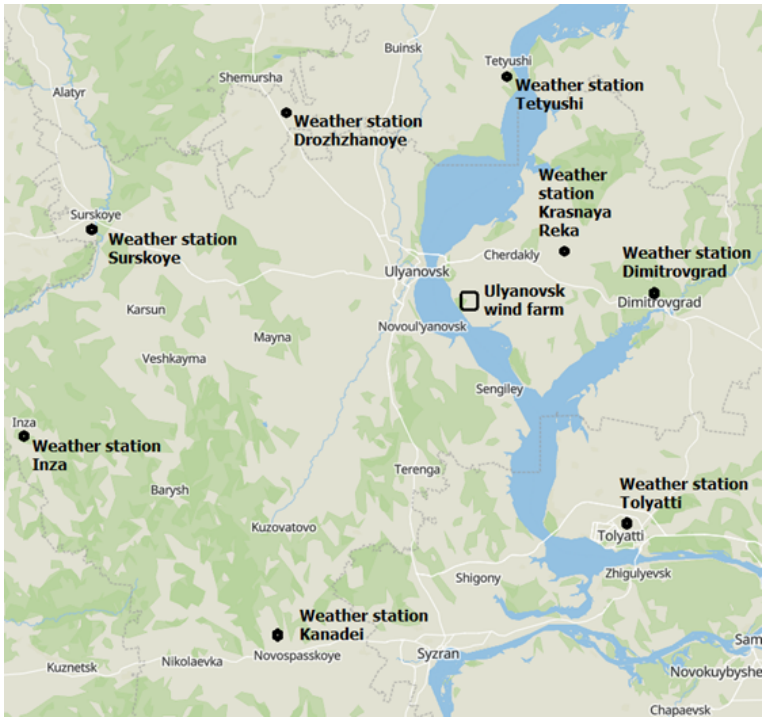

Figure 3. Weather study area [50], with weather stations [49].

Using archival data from weather stations for 2022, systematized input variables were prepared with a time interval of one hour. Archival data from the Ulyanovsk weather station, which is closest to the wind farm, was used as output variables for training. The safe and efficient operation of wind farms largely depends on meteorological conditions.

As modern research shows, the processes of formation of dangerous weather phenomena are accompanied by physical effects that locally manifest themselves in the terrestrial spheres, which are usually called harbingers of events. Based on the characteristics of these harbingers, one can judge the magnitude of a future probable event. Significant phenomena affecting the safety and operation of wind farms include strong winds—this is a squat wind with a speed of more than 15 m/s; blizzards are the transfer of snow masses over the surface of the earth by gusty and strong winds, the speed of which is at least 15 m/s with visibility less than 500 m; heavy rains are heavy precipitation with an intensity of more than 30 mm per day; hail—solid precipitation with a deposit diameter of 5 to 20 mm; squalls—horizontal whirlwinds with wind speeds exceeding 15 m/s; icing—deposits of water and ice on the surface with a deposit diameter of at least 50 mm [51].

2.4. Training Process

The PyTorch library in Python was used for training. During training, the following training parameters were set:

- Training set: 98,110 samples (70% data);
- Test set: 42,050 samples (30% data);
- Optimizer: Pytorch Adam;
- Loss function: Pytorch Binary Cross Entropy;
- Learning rate epoch: 0.0001;
- Batch size: 20;
- Epochs: 1200.

The training process, where there is a decrease in the error in terms of Binary Cross Entropy [52] at each training epoch, is shown in Figure 4. When training a neural network, the error decreases at each iteration. The number of iterations was chosen empirically when the required degree of learning was achieved.

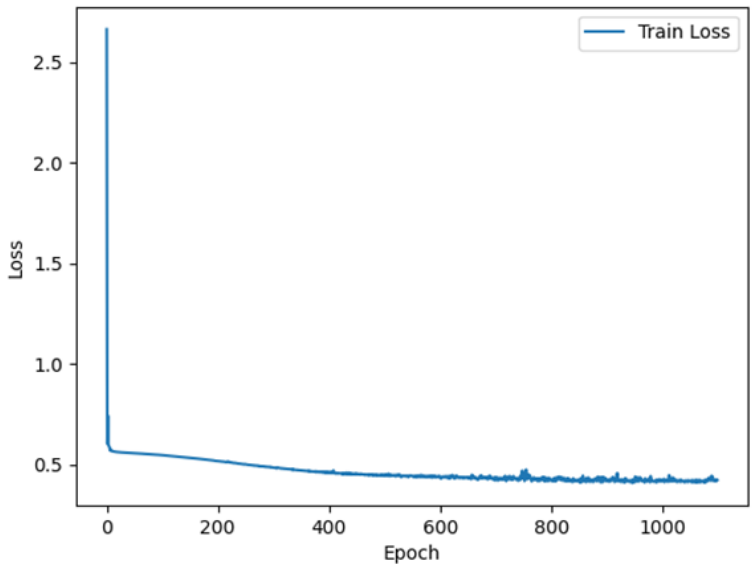

Figure 4. A neural network training.

A sufficient level of quality of the proposed model is observed after 1000 years of training. After training on the test set, the results presented in Figure 5 were obtained. The results are presented in the form of an error matrix, which shows that the model works quite accurately. The level of overall accuracy was 81.78%, macro-average recall was 81.07% and macro-average precision was 75.05%. For multi-class classification, macro-average recall and macro-average precision are calculated as:

$$MacroAverageRecall = \frac{\sum_{k=1}^{K} Recall_k}{K} \tag{3}$$

$$MacroAveragePrecision = \frac{\sum_{k=1}^{K} Precision_k}{K} \tag{4}$$

where K is the total number of classes, $Recall_k$ is the recall for each class, $Precision_k$ is the precision for each class. $Recall_k$ and $Precision_k$ are calculated by the formulas:

$$Recall_k = \frac{TP_k}{TP_k + FN_k} \tag{5}$$

$$Precision_k = \frac{TP_k}{TP_k + FP_k} \tag{6}$$

where TP_k are true positive elements that are predicted correctly, FN_k are false negative elements that belong to class k but were classified as another class (columns in the error matrix), and FP_k are false positive elements that do not belong to class k, but were assigned to this class (rows in the error matrix).

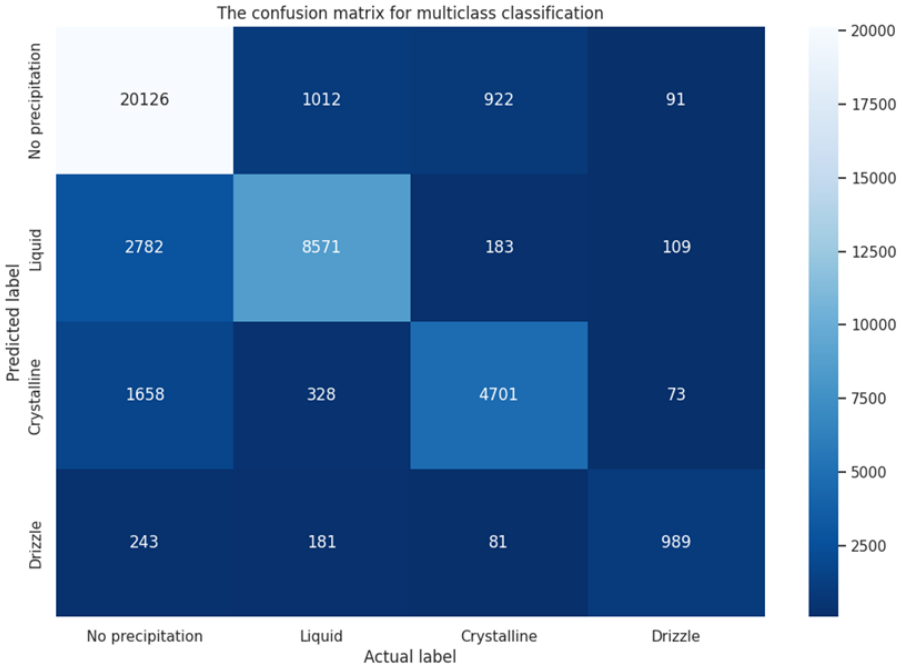

Figure 5. Error matrix for weather-classification model.

To check the quality of the neural network model, it was compared with other machine learning methods in classification tasks, such as boosting (XGBoost), random forest (RF), and the support vector machine (SVM) method. The results of the comparison are shown in Table 1.

Table 1. Comparison of machine learning methods in classification tasks.

Model	Accuracy	Macro-Average Recall	Macro-Average Precision
Neural network	81.78%	81.07%	75.05%
XGBoost	79.13%	74.73%	72.14%
RF	77.63%	71.61%	70.64%
SVM	77.13%	70.80%	70.14%

As can be seen from the results, the neural network model showed the best results, which is due to its nonlinearity in making a forecast. Based on this, a decision was made on its further use in solving the task set.

An interface in the form of an interactive map has been developed to visualize the work of a neural network. The size of the circle corresponds to the probability of the precipitation class; the larger the diameter of the circle, the higher the probability. The colors determine the precipitation class: orange—no precipitation; green—precipitation in liquid form; blue—crystalline precipitation; purple—drizzle, fog. The result of the neural network based on forecast data from weather stations is presented in Figure 6.

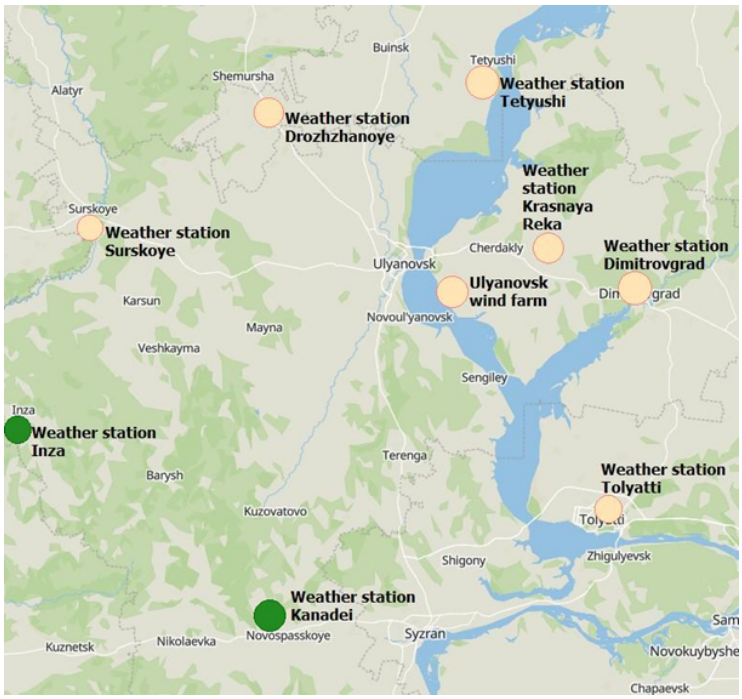

Figure 6. Precipitation formation zones.

The developed neural network is a part of the analytical module, which allows you to make decisions about the use of control actions in the form of injections of moisture concentrators. The analytical module consists of production rules, which, based on the data received in them, form a logical conclusion in the form of decisions on the impact on the meteorological situation. An example of the rules is given below:

If dew point<0 AND Precipitation type="Rain" THEN
Solution="Inject moisture concentrator"
End
If dew point>0 AND Precipitation type="No precipitation" THEN
Solution="Do nothing"
End

It is possible to increase the accumulation of expert rules and improve the accuracy of decisions made when influencing the meteorological situation. This approach also allows you to achieve the necessary accuracy in decision making, without the use of large computing centers, which may be required when running large modern models for forecasting weather conditions, such as GraphCast [53]. The considered neural network has registration certificate No. 2023663950 dated 2023 "Neural network for classification of zones of probable precipitation formation".

3. Numerical Methods

3.1. ABL Modeling

Simcenter STAR-CCM+ software (version 2022.1) is used to simulate the ABL and create a digital model of the wind turbines and terrain. The developed approach using machine learning allows studying weather phenomena based on data from weather stations in the vicinity of wind turbines and classifying meteorological events. This will allow the creation of a knowledge base of climatic features and preparation of input data for CFD modeling.

Numerical simulation is based on the finite volume method (FVM) and the Navier–Stokes equation. Iterative calculations are performed for the velocity and pressure fields using an algebraic multigrid (AMG) linear solver. STAR-CCM+ is launched using a LES turbulence model with built-in software functions. In the LES model, large-scale turbulence is directly resolved throughout the flow domain and small-scale motions are modeled [54]. The error in the turbulence modeling assumptions is not so significant when modeling "less" turbulence and explicitly solving for most of it. In addition, it is assumed that small-sized vortices are similar and thus amenable to simpler and more universal models. The disadvantage of this approach is the computational cost, which, although less than with direct numerical modeling, is nevertheless large. In cases of studying the boundary layer in the area of wind farms, LES allows you to solve a more detailed problem and take into account factors from small eddies. Unlike RANS equations, the equations that are solved for LES are obtained using spatial filtering rather than an averaging process. Each decision variable φ is decomposed into a filtered value $\tilde{\varphi}$ and a filtered value φ', or subgrid value:

$$\varphi = \tilde{\varphi} + \varphi' \tag{7}$$

where φ represents velocity components, pressure, energy, or species concentration.

Inserting the decomposed solution variables into the Navier–Stokes equations results in equations for the filtered quantities. The filtered equations are rearranged into a form that looks identical to the unsteady RANS equations. However, the turbulent stress tensor now represents the subgrid scale stresses. These stresses result from the interaction between the larger, resolved eddies and the smaller, unresolved eddies and are modeled using the Boussinesq approximation as follows:

$$T_{SGS} = 2\mu_t S - \frac{2}{3}(\mu_t \nabla \tilde{v}) \tag{8}$$

where μ_t is the subgrid scale turbulent viscosity; S is the mean strain rate tensor and computed from the resolved velocity field; $\tilde{v}$ is the filtered velocity. LES requires closure of the filtered Navier–Stokes equations by modeling the subgrid-scale stress tensor. The subgrid scale model provides a formula for the subgrid scale viscosity μ_t in the Boussinesq approximation for the subgrid scale stress tensor. A dynamic scale model of the Smagorinsky subnetwork is available in STAR-CCM+ [55,56] with a common basic form as the Smagorinsky model. A special feature of the approach is the ability to calculate a locally time-varying modular coefficient by test filtering the flow field. This dynamic change allows the correct result to be calculated for wall-confined flows with complex geometries. Based on the scale of the Ulyanovsk wind farm, the Coriolis effect was not taken in this work. Similar research conditions are presented in the work [57].

3.2. Wind Turbine Model

A wind turbine extracts mechanical energy from the kinetic energy of the wind. It acts as a actuator disk, changing the wind speed from U_0 to U in the rotor plane and further slowing it down to U_1 in the wake. To model the impact of wind turbine operation, the 1D Momentum Method included in STAR CCM+ was used. A special feature of the approach is the addition of an initial term to the momentum equations to simulate the effects of a wind turbine. The original term takes into account both the axial and tangential effects created by an ideal Horizontal Axis Wind Turbine (HAWT) with wake rotation. The

induced speed on the rotor consists of an axial component a and a tangential component a' acting in the plane of the rotor. The model is based on the use of annular stream tube with a certain radius r and thickness dr. Figure 7 schematically shows the virtual disk of a wind turbine.

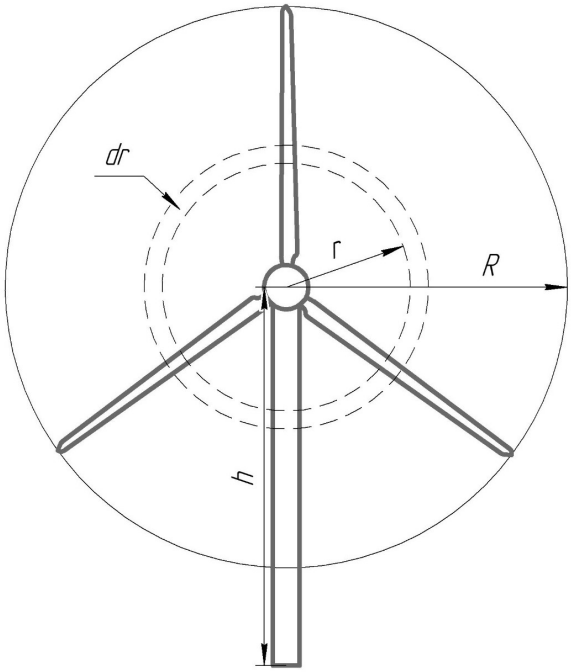

Figure 7. Structure model of wind turbine.

The cross-sectional area can be determined by the dependence based on this representation of the virtual disk:

$$dA = 2\pi r dr \tag{9}$$

This approach makes it possible to duplicate the wind turbines with high accuracy, while significantly reducing the calculation time and requirements for computing resources, which is especially important when modeling wind farms. Knowing the specific geometric characteristics of wind turbines, the thrust coefficient and the dependence of the rotations on the wind speed, the use of a virtual disk becomes the best tool for conducting research work. Under the influence of wind force, the flow is distributed over the surface of the disk and penetrates it, which is described by the following expression, which determines the total thrust of the wind turbine:

$$F_T = \frac{1}{2}\rho C_T U_\infty^2 2\pi r dr \tag{10}$$

where ρ is the air density, C_T is the thrust coefficient, U_∞ is the velocity, D diameter.

Using the built-in 3D CAD tool STAR-CCM+, towers and wind turbine nacelles were created using the geometric characteristics of wind turbines operated at Ulyanovsk wind farm. Wind turbines are located in the computational area according to satellite imagery data. The configuration of the physical models of virtual disks took into account the thrust coefficients and the dependencies of the rotor speed and power on wind speed.

4. Verification and Numerical Study of the Movement of Air Masses in the Wind Farm Area

4.1. Wind Turbine Model Verification

Numerical study of the ABL was carried out to study in detail the processes occurring in the area of wind turbines. The first stage of the research was to analyze the adequacy of

the model on an autonomous wind turbine. The results in Figure 8 were compared with the researchers' experimental data [58].

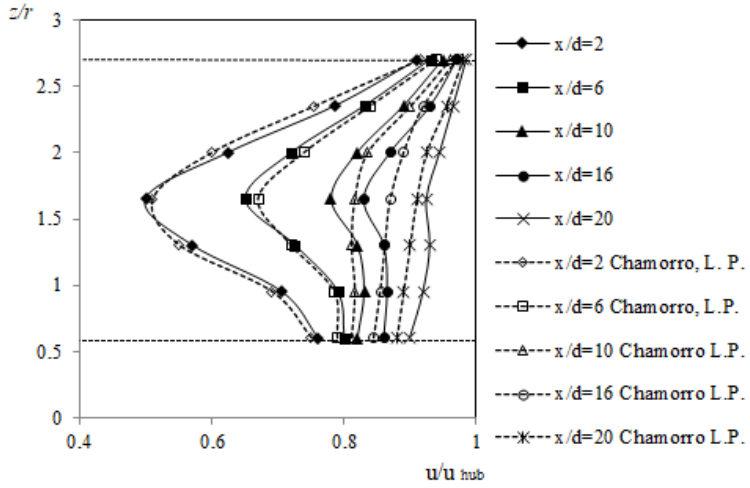

Figure 8. Vertical profiles of the time-averaged streamwise velocity [58]: solid line—results of CFD modeling using the proposed approach; dotted line—results obtained by Chamorro L.P.

A digital model of the V126-3.45 wind turbine was developed based on available data [59] in the computational domain of 20D, 12D, and 2.5D in the downstream (x), spanwise (y), and perpendicular to the wall (z) directions, respectively (D is the rotor diameter). The initial conditions were set taking into account the recommendations in [58]. The speed of the undisturbed flow was U_∞ = 10 m/s. The Neumann boundary condition is used at the outlet wall. The grid requirements were as follows: for grid G1, 10 grid nodes are uniformly distributed per one rotor diameter in all three directions, which are 20 and 30 for grid G2 and G3, respectively. The grid nodes are uniformly distributed in the vertical and spanwise directions. In the streamwise direction, the grid is uniform from inlet to 12D downstream and then stretched to the outflow boundary. The induction factor is 0.15. Since the induction factor cannot be directly extracted from the wind tunnel measurements, this induction factor is computed from a separate (LES) with actuator line model, in which we specify the tip-speed ratio which can be obtained from the wind tunnel measurements [60]. Figure 9 shows 11 sections of interest. The first section is at the entrance to the computational domain, the subsequent ones are located equidistantly, at a distance of 2D.

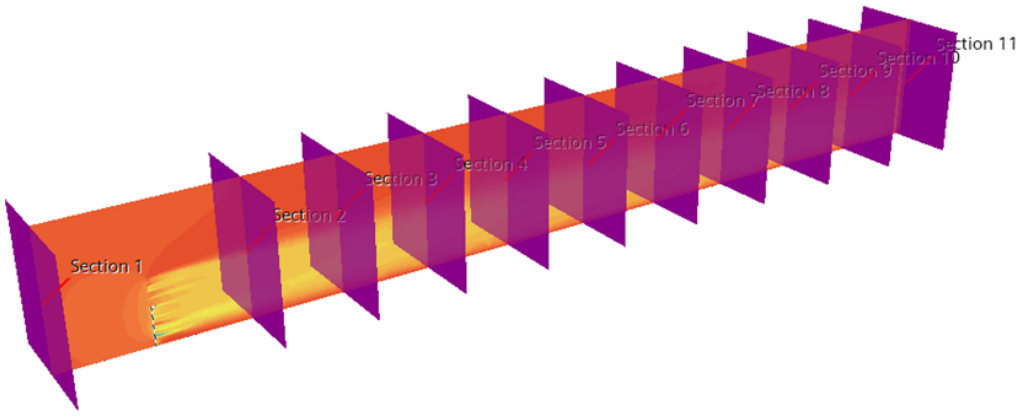

Figure 9. Plane sections of the computational domain.

Velocity profiles were calculated, and are in good agreement with the results in Figure 8. Figure 10 shows the velocity distribution in the computational domain behind the wind turbine.

Figure 10. Speed distribution scene in the computational domain behind the simulated wind turbine.

Based on the comparative analysis, it can be noted that the calculation error is less than 5%.

4.2. Numerical Study of the Movement of Air Masses in the Wind Farm Area

The studies were carried out in a large computational domain in which the flow around a wind power plant was simulated. Using the built-in STAR CCM+ tools, models of the masts and nacelles of the Vestas V126-3.45 MW [59] wind turbines operated at the Ulyanovsk wind power plant were developed. A polyhedral mesh with refinement in the area of wind turbines was used. Figure 11 shows the scene of the computational domain in the wind farm area, highlighting the boundary conditions: inlet is the area of entry of air masses with specified conditions; outlet—area of exit of air masses; walls 1 and 2—side walls, "Symmetry Plane" type; the top of the calculation area also had a "Symmetry Plane" function. The lower part of the calculation area has the "Impenetrable wall" function and duplicates the terrain in the wind farm area.

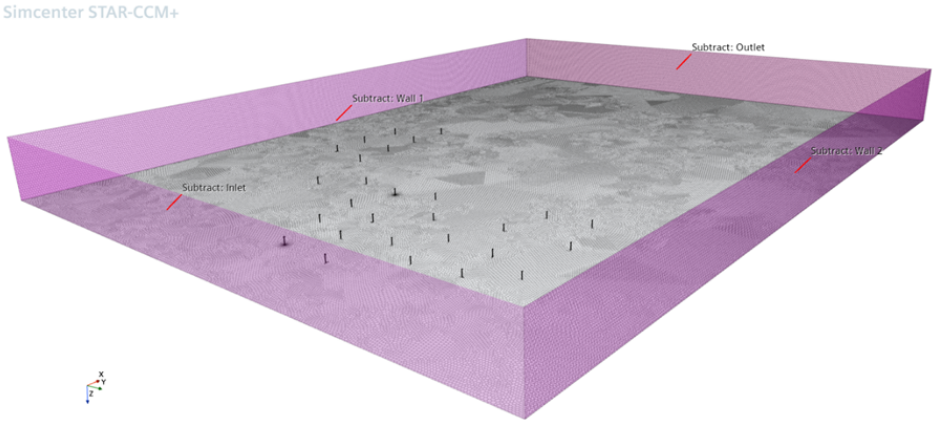

Figure 11. Wind farm computational domain.

Based on the research conditions and limitations of the computational area of the program, the model was scaled and reduced by 10 times, taking into account the theory of similarity [61]. In the virtual disk area, the grid size was set to 0.01 m, in the near wake area to 0.08 m, and the base grid size was 0.3 m. To construct a volumetric mesh, cells with a polyhedral shape were used—polyhidral. The choice of mesh, justification for quality, and approach to construction are described in [45,62]. The total number of cells in the computational domain was 146,268,742. To carry out the calculations, three calculation servers were combined into a calculation cluster; as a result, the use of 182 cores out of 192 available was achieved.

The computational area was limited to 10 km along the x-axis, 10 km wide along the y-axis, and 1 km high along the z-axis. For the calculations, models of the wind farm were prepared and built on eight cardinal points. Considering the similarity requirement, the dimensions were reduced 10 times. The obtained results of the numerical studies in this

work are reduced to normal physical values without considering the similarity number. The following data were used as initial conditions for the calculation: wind speed, m/s; wind direction, cardinal points (WNW, NNW, NNE, ENE, ESE, SSE, SSW, WSW); air temperature (°C); atmospheric pressure (hPa); and precipitation amount (mm). The values of these parameters are determined by the program module responsible for preparing the initial conditions based on data received from weather stations. The wind speed on the input side was set to profile according to the requirements of the standard [63]. The wind speed was increased 10 times based on the requirements of the similarity theory. The upper and side walls of the computational area were slipped, and the bottom wall imitated the real surface on the earth with a given roughness to increase the friction coefficient Cf = 0.008 [64]. The physical time for each calculation was limited from 800 s to 2400 s, depending on the wind speed. The time value was determined based on the conditions of the specified flow velocity in the computational domain and the conditions for the stabilization of the turbulent flow behind the wind farm.

The layout of the wind farm and the characteristics of the area where the wind farm is located are presented in [45]. These results do not take into account the yaw system of the wind turbines and for each calculation the direction of the wind turbines was the same.

In order to study the movement of air masses in the area of the wind farm and study the distribution of the turbulent wake behind the wind farm and its influence on the ABL, research was carried out in two directions, southern and eastern. Figure 12 shows speed profiles for the eastern wind, along a section along the surface at an altitude of 110 m.

The developed approach allows us to study the movement of air masses in the area of wind turbines and analyze traces of shading, which will allow the effective placement of wind turbines when designing a wind power plant, as well as predict the wind energy potential.

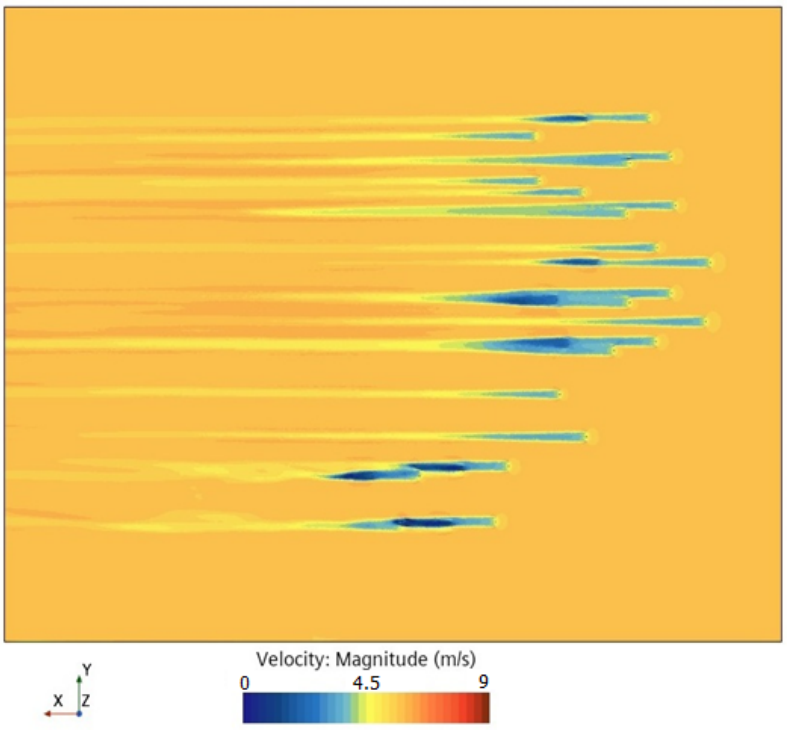

(**a**)

Figure 12. *Cont.*

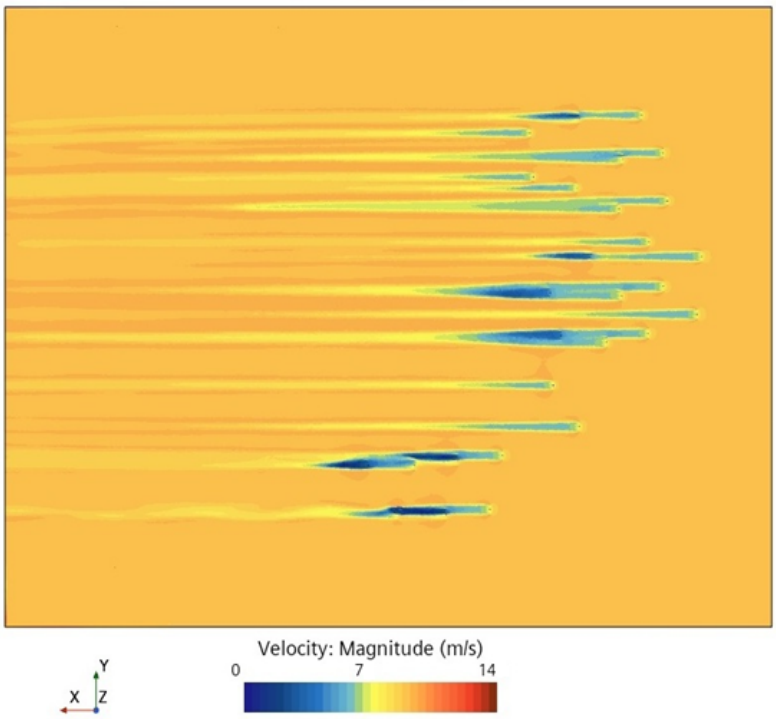

(**b**)

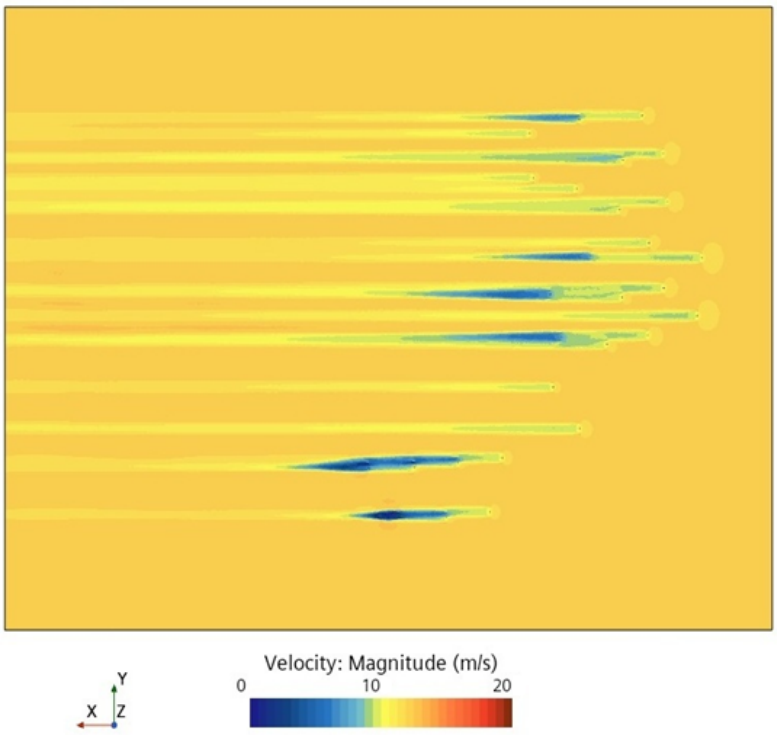

(**c**)

Figure 12. Velocity profile for eastern wind direction: (**a**) wind speed 6 m/s; (**b**) wind speed 9 m/s; (**c**) wind speed 12 m/s.

The velocity profiles for 6 m/s, 9 m/s, and 12 m/s eastern wind input conditions were plotted at a height of 110 m from the surface for a detailed analysis (see Figure 13). Using the built-in Star-CCM+ functions [54], plots were generated to show the velocity deficit, and the results are presented in Figure 14a–c.

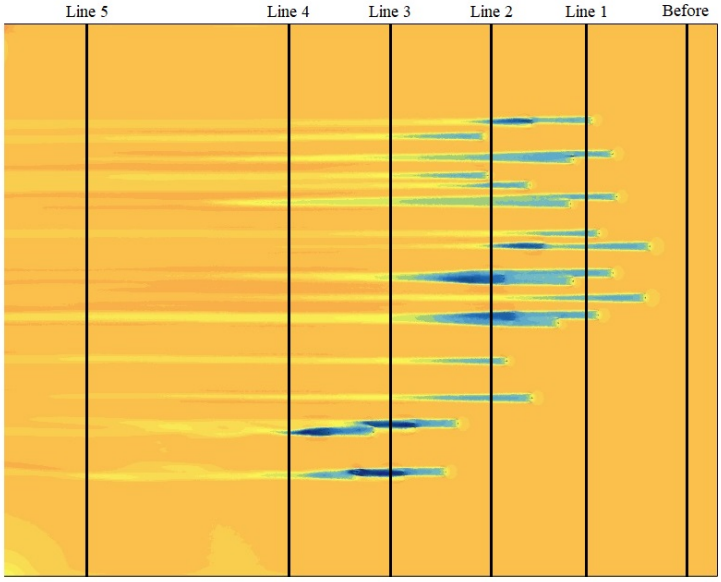

Figure 13. Data lines across the wind farm in the computational domain for easterly wind direction.

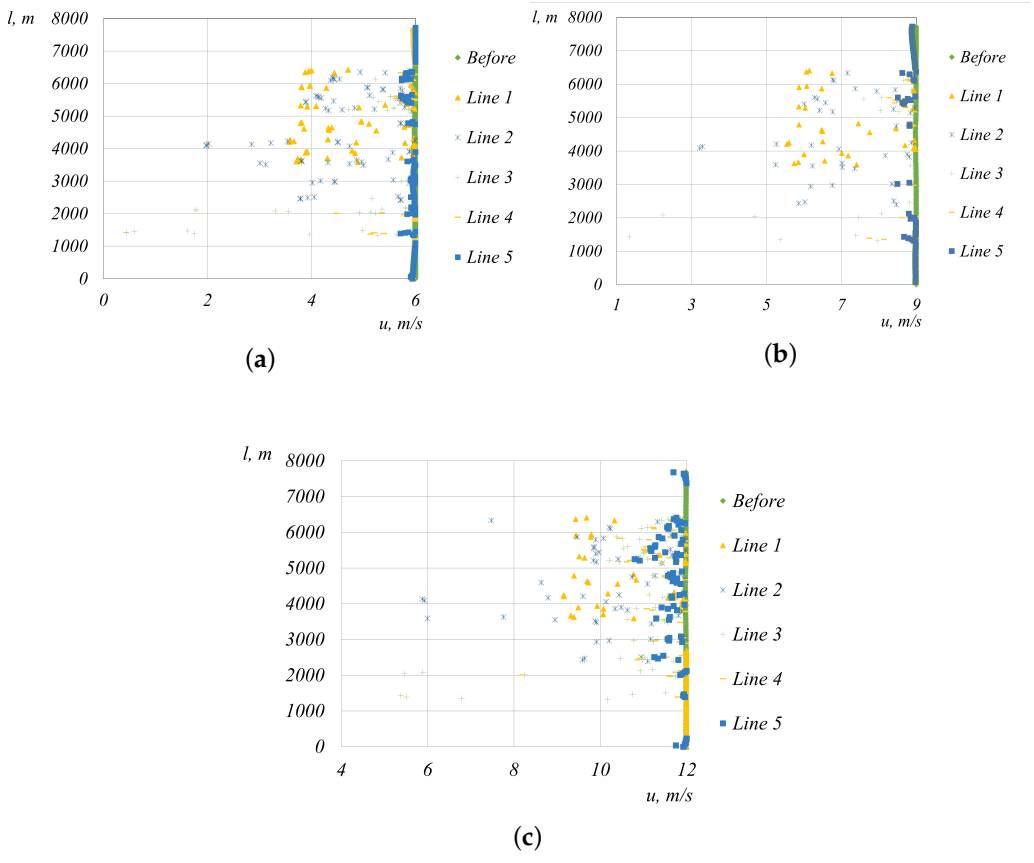

Figure 14. Wind farm area velocity deficit with eastern wind direction: (**a**) wind speed 6 m/s; (**b**) wind speed 9 m/s ; (**c**) wind speed 12 m/s.

A significant overlap of the wind turbine wakes and an increase in the velocity deficit in the wind farm area significantly reduces the wind farm efficiency. The maximum reduction in velocity was observed in areas where the wind turbines were most densely located. The induced velocity deficit of a group of wind turbines was clearly expressed in the far wake and extended to the end of the computational domain. The figures also show differences in the wake turbulence for similar groups of wind turbines, which may

be due to the low wind speed and high intensity of turbulence caused by the terrain. The difference in height was 22 m in the wind farm area [45]. At a wind speed of 12 m/s, the average value of the velocity deficit behind the wind farm was 0.47 m/s, corresponding to line 10 in Figure 14. Line 10 is approximately 4 km from the last wind turbine. At a wind speed of 9 m/s, the average value of the velocity deficit behind the wind farm is 0.21 m/s, corresponding to line 10 in Figure 14b. At a wind speed of 6 m/s, the average value of the velocity deficit behind the wind farm was 0.12 m/s, corresponding to line 10 in Figure 14.

A data line was constructed at a height of 110 m from the surface for a detailed consideration of the near and far wake behind a group of wind turbines in the computational domain (see Figure 15).

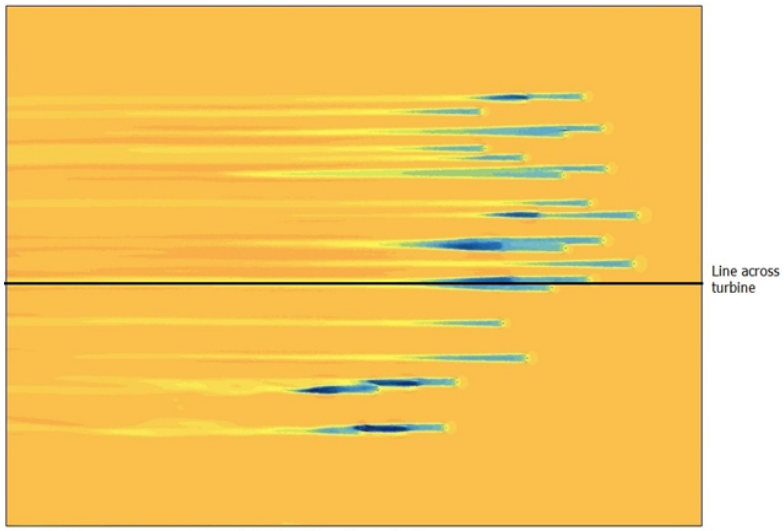

Figure 15. Data line along a group of wind turbines in the computational domain for easterly wind direction.

Plots of velocity deficit behind a group of three wind turbines for speeds of 6, 9, 12 m/s and eastern wind direction were generated using the built-in Star-CCM+ functions; the results are presented in Figure 16a–c.

Figure 16 shows a significant influence of wind turbines on the velocity in the near and far wake. It should be noted that behind a group of wind turbines at a wind speed of 12 m/s the far wake in the computational domain is not completely restored. At a distance of 10 km from the beginning of the computational domain, the maximum velocity deficit is 0.96 m/s. For wind speeds of 9 m/s and 6 m/s, the velocity deficit at the boundary of the computational domain is less pronounced.

The results of CFD modeling of the movement of air masses in the wind farm area were obtained using machine learning methods and prepared by the program module responsible for preparing the initial conditions "Software module for automated preparation of initial data for a digital twin of a wind turbine", registration certificate No. 2022665200 dated 2022. The presented results of the movement of air masses and velocity profiles in the area of the wind farm allow us to assess the speed deficit and restoration of the turbulent wake, which makes it possible to predict the operating mode of wind turbines and their efficiency. To evaluate the possibility of modeling the movement of air masses in the area of a wind farm, the results for different wind directions were presented. Figure 17 shows the velocity profiles for the southern wind direction, along a plane section at an altitude of 110 m.

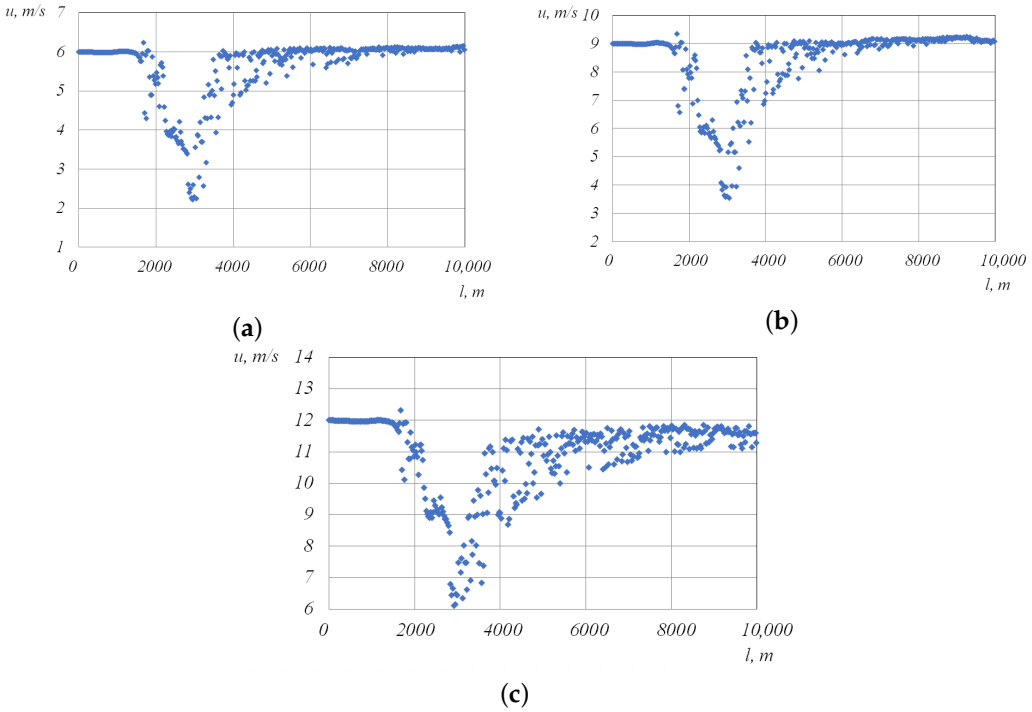

Figure 16. Velocity deficit for a group of wind turbines with eastern wind direction: (**a**) wind speed 6 m/s; (**b**) wind speed 9 m/s ; (**c**) wind speed 12 m/s.

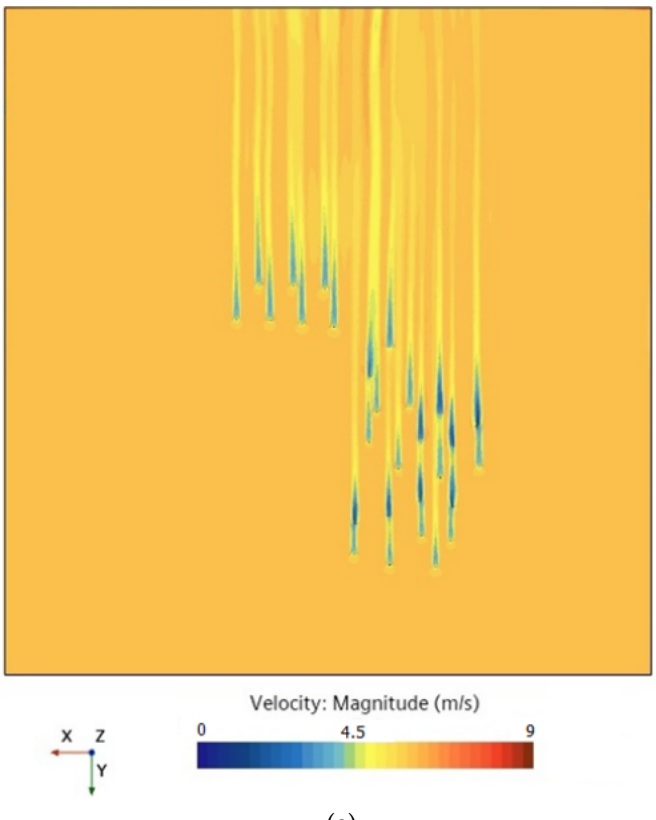

(**a**)

Figure 17. *Cont.*

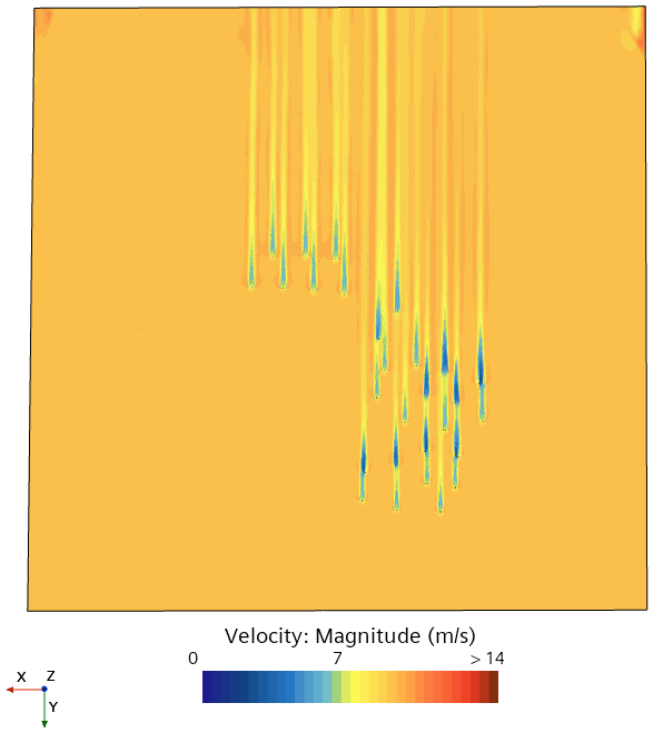

(**b**)

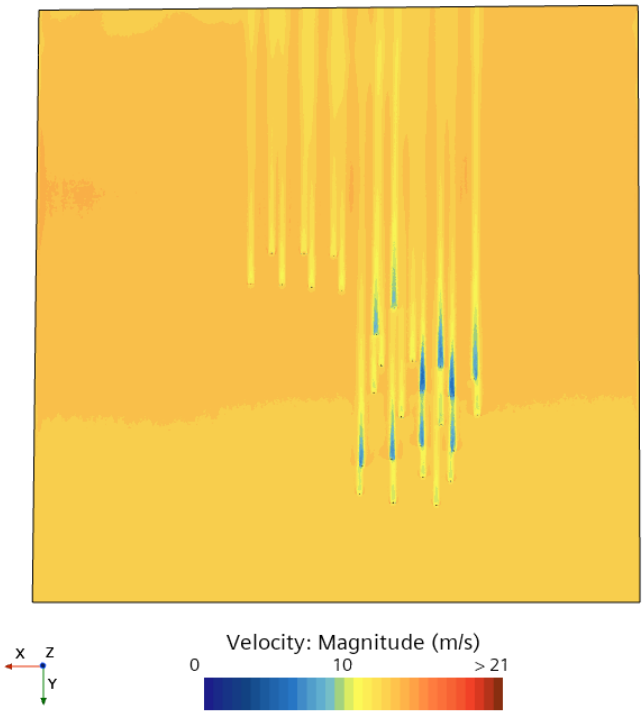

(**c**)

Figure 17. Velocity profile for southern wind direction: (**a**) wind speed 6 m/s; (**b**) wind speed 9 m/s; (**c**) wind speed 12 m/s.

For a detailed examination of the velocity profiles with a southerly wind direction, data lines were constructed in the computational domain at a height of 110 m from the surface (see Figure 18). Using the built-in Star-CCM+ functions, plots were generated for the velocity deficit behind the wind farm for wind speeds of 6, 9, 12 m/s for the southern wind direction; the results are in Figure 19a–c.

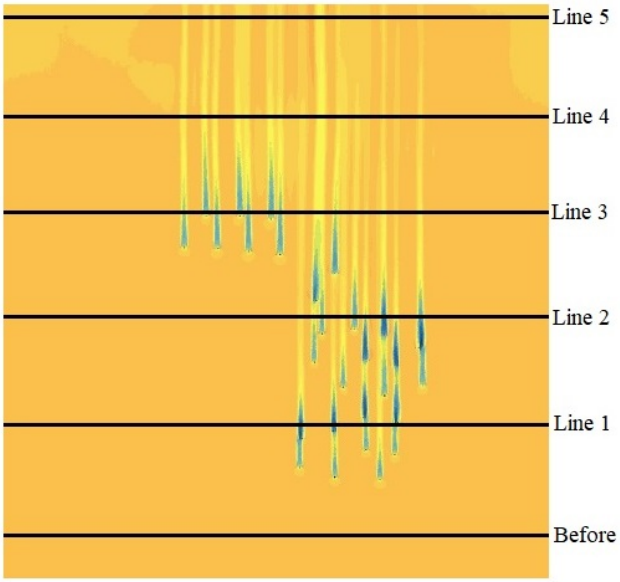

Figure 18. Data lines across the wind farm in the computational domain for southerly wind direction.

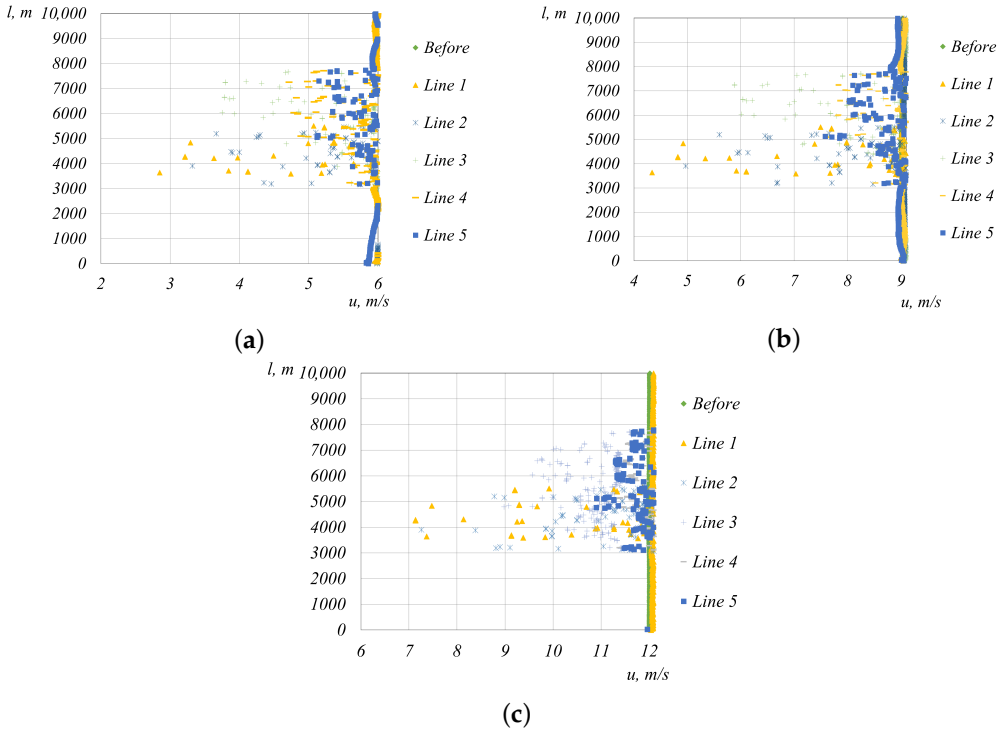

Figure 19. Velocity deficit behind the wind farm for eastern wind direction: (**a**) wind speed 6 m/s; (**b**) wind speed 9 m/s; (**c**) wind speed 12 m/s.

It should be noted that the shading effect of wind turbines is less pronounced due to the specific layout of the wind farm. The induced velocity deficit of a group of wind turbines is clearly expressed in the far wake with a tunnel arrangement of wind turbines. The figures also show differences in wake turbulence for similar groups of wind turbines, which may be due to the low wind speed and high intensity turbulence caused by the terrain. At a wind speed of 12 m/s, the average value of the velocity deficit behind the wind farm is 0.47 m/s, corresponding to line 9 in Figure 19a. Line 9 is approximately 3 km from the last wind turbine. At a wind speed of 9 m/s, the average value of the velocity deficit behind the wind farm is 0.31 m/s, corresponding to line 9 in Figure 19. At a wind

speed of 6 m/s, the average value of the velocity deficit behind the wind farm is 0.2 m/s, corresponding to line 9 in Figure 19.

A longitudinal data line was constructed at an altitude of 110 m from the surface to consider the near and far wake behind a group of wind turbines in the computational domain (see Figure 20).

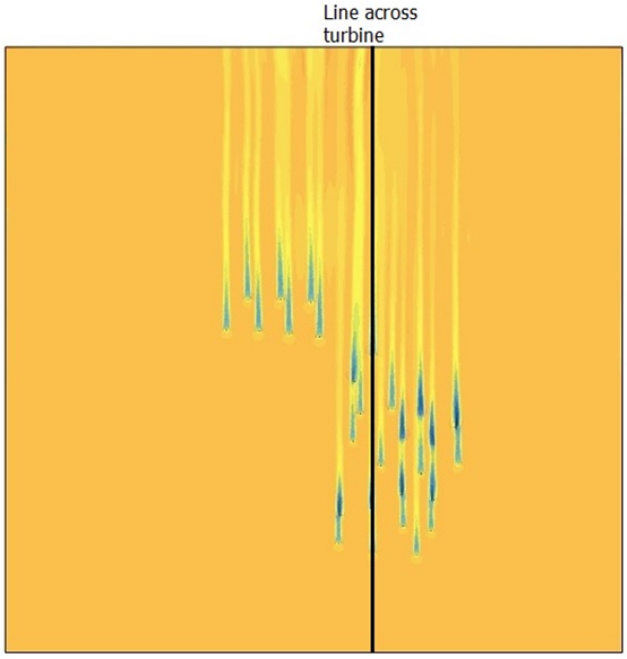

Figure 20. Longitudinal data line for a group of wind turbines in the computational domain for the southern wind direction.

The plots of velocity deficit behind a group of three wind turbines for wind speeds of 6, 9, 12 m/s with a southerly wind direction were generated using the built-in Star-CCM+ functions. The results are presented in Figure 21a–c.

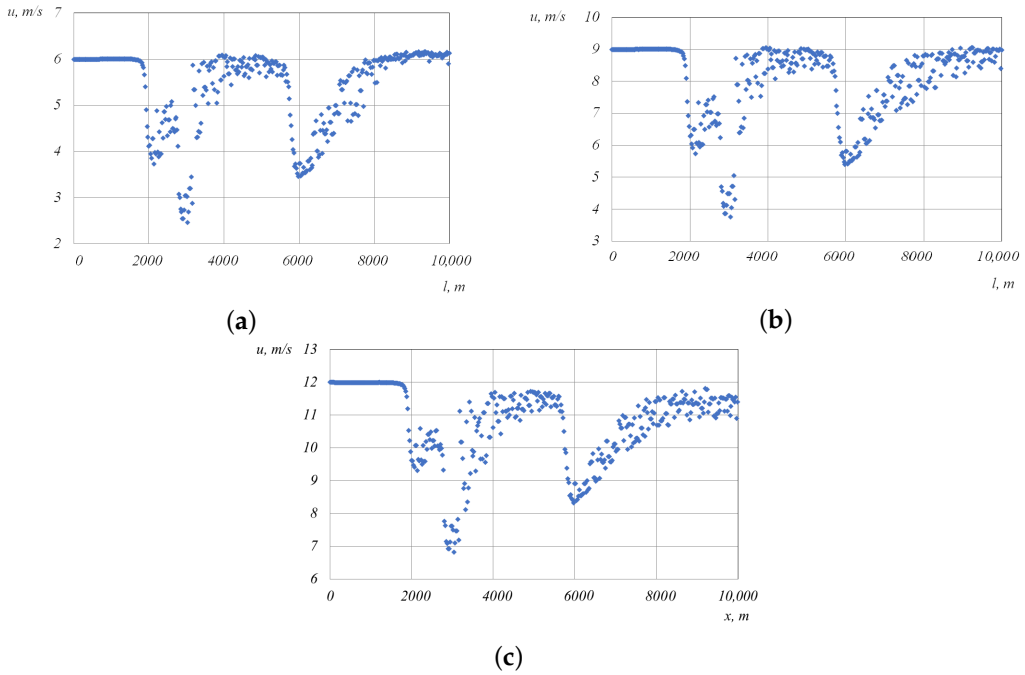

Figure 21. Velocity deficit behind a group of wind turbines with a southern wind direction: (**a**) wind speed 6 m/s; (**b**) wind speed 9 m/s; (**c**) wind speed 12 m/s.

These results show the effectiveness of the distant locations of the wind turbines in the wind farm area. It should be noted that behind a group of wind turbines at a wind speed of 12 m/s, the far wake in the computational domain was not completely restored. At a point 1000 m from the beginning of the computational domain, the velocity deficit for these conditions was 1.1 m/s. At a wind speed of 9 m/s, the velocity deficit was reduced to 0.68 m/s. At a wind speed of 6 m/s, the velocity at the boundary is restored.

Analyzing the results of Figures 16 and 21, we note the influence of different wind turbine-placement schemes. When designing wind farms, in our opinion, the optimal distance between wind turbines should be at least 1200 m. At distances of 300–500 m (as in Figure 16), we can obtain a deeper speed deficit, which leads to a longer recovery. At distances of 500–1000 m (as in Figure 21 between the first and second wind turbines), the speed deficit is smaller, and recovery is faster.

The proposed approach enables the assessment of the speed deficit and recovery of the turbulent wake. Based on the obtained data, it is possible to predict the operating modes of wind turbines by considering meteorological phenomena. The above research methods were implemented in the form of software products for which certificates of state registration were obtained: "Software module for automated preparation of initial data for a digital twin of a wind turbine," registration certificate No. 2022665200 dated 2022, and registration certificate "Neural network for classification of zones of probable precipitation formation" No. 2023663950 dated 2023.

5. Conclusions

This article presents a hybrid approach to study the movement of air masses in the field of wind power, based on the use of a multilayer neural network and CFD modeling. In the example of the Ulyanovsk wind farm, weather characteristics were monitored, a neural network was trained, and an analytical module consisting of production rules was configured, which, based on the data obtained from them, formed a logical conclusion in the form of decisions on the impact on the meteorological situation. During training, a general accuracy of 81.78%, macro-average recall of 81.07%, and macro-average precision of 75.05% were achieved. The proposed solution also allows for the creation of initial conditions for CFD modeling. This study presents a model of the movement of air masses in a wind farm area with a modeling error of less than 5%. Digital models of the relief and wind turbines of the Ulyanovsk Wind Farm were created using the Simcenter STAR-CCM+ CFD software package, version 2022.1. An approach based on the LES model using the actuator model of the drive disk (ADM) was implemented for modeling. The results of modeling the movement of air masses in the wind farm area for speeds ranging from 6 to 12 m/s in the south and east wind directions were obtained. Figures of the movement of air masses are presented, and velocity profiles in the area of the wind farm are constructed, allowing the assessment of the speed deficit and restoration of the turbulent wake. Local speed deficit zones for groups of wind turbines have been identified, which reduce the energy-generation efficiency. The developed solutions will make it possible to effectively design wind farms by considering the many factors of air mass movement and meteorological phenomena.

Author Contributions: Conceptualization, V.N.K. (Vladislav N. Kovalnogov), R.V.F. and A.V.C.; methodology, V.N.K. (Vladimir N. Klyachkin), R.V.F. and V.P.T.; software, V.N.K. (Vladimir N. Klyachkin) and D.A.D.; validation, V.N.K. (Vladimir N. Klyachkin), D.A.D. and A.V.C.; investigation, V.N.K. (Vladislav N. Kovalnogov), R.V.F. and A.V.C.; writing—original draft preparation, V.N.K. (Vladislav N. Kovalnogov), V.P.T. and A.V.C.; writing—review and editing, V.N.K. (Vladislav N. Kovalnogov), R.V.F. and A.V.C.; visualization, D.A.D., A.V.C.; supervision, V.N.K. (Vladislav N. Kovalnogov); project administration, V.N.K. (Vladislav N. Kovalnogov); funding acquisition, V.N.K. (Vladislav N. Kovalnogov). All authors have read and agreed to the published version of the manuscript.

Funding: The study was supported by the Russian Science Foundation grant No. 22-19-00030, https://rscf.ru/project/22-19-00030/ (accessed on 31 July 2024).

Data Availability Statement: Data are contained within the article.

Acknowledgments: The study was performed at the Laboratory of Interdisciplinary Problems in Energy Production of the Ulyanovsk State Technical University, established with the support of the megagrant of the Government of the Russian Federation (Contract No. 075-15-2021-584).

Conflicts of Interest: The authors declare no conflicts of interest.

Abbreviations

The following abbreviations are used in this manuscript:

ABL	atmospheric boundary layer
CFD	computational fluid dynamics
ADM	actuator disk model
LSTM	long short-term memory
CNN	convolution neural network
NWP	numerical weather prediction
ANN	artificial neural network
RANS	Reynolds-averaged Navier–Stokes
LES	large eddy simulation
HFM	high fidelity modeling
BRM	blade resolution models
SOWFA	simulator for wind farm applications
SGS	subgrid scales
ML	machine learning
ReLU	rectified linear unit
FVM	finite volume method
AMG	algebraic multigrid
HAWT	horizontal axis wind turbine

References

1. Chin, C.S.; Peh, C.M.; Venkateshkumar, M. *Modeling and Simulation of Offshore Wind Farms for Smart Cities*; IntechOpen: London, UK, 2020. Available online: https://www.intechopen.com/chapters/67839 (accessed on 31 July 2024).
2. Kudelin, A.; Kutcherov, V. Wind ENERGY in Russia: The current state and development trends. *Energy Strategy Rev.* **2021**, *34*, 100627. (In Russian) [CrossRef]
3. Tsai, W.-C.; Hong, C.-M.; Tu, C.-S.; Lin, W.-M.; Chen, C.-H. A Review of Modern Wind Power Generation Forecasting Technologies. *Sustainability* **2023**, *15*, 10757. [CrossRef]
4. Shi, X.; Chen, Z.; Wang, H.; Yeung, D.Y.; Wong, W.-K.; Chun Woo, W. Convolutional lstm network: A machine learning approach for precipitation now casting. *arXiv* **2015**, arXiv:1506.04214. [CrossRef]
5. Mehrkanoon, S. Deep shared representation learning for weather elements forecasting. *Knowl.-Based Syst.* **2019**, *179*, 120–128. [CrossRef]
6. Hewage, P.; Trovati, M.; Pereira, E.; Behera, A. Deep learning-based effective fine-grained weather forecasting model. *Pattern Anal. Appl.* **2021**, *24*, 343–366. [CrossRef]
7. Lira, H.; Martí, L.; Sanchez-Pi, N. A Graph Neural Network with Spatio-Temporal Attention for Multi-Sources Time Series Data: An Application to Frost Forecast. *Sensors* **2022**, *22*, 1486. [CrossRef] [PubMed]
8. Shouman, E.R.M. *Wind Power Forecasting Models. Wind Turbines—Advances and Challenges in Design, Manufacture and Operation*; IntechOpen: London, UK, 2022. Available online: https://www.intechopen.com/chapters/81755 (accessed on 31 July 2024).
9. Rekioua, D.; Rekioua, T.; Elsanabary, A.; Mekhilef, S. Power Management Control of an Autonomous Photovoltaic/Wind Turbine/Battery System. *Energies* **2023**, *16*, 2268. [CrossRef]
10. Radkevich, M.V.; Shipilova, K.B.; Khamidov, A.O.; Razzakov, R.I.; Gapirov, A.D. Review of local climate control capabilities. *Univers. Chem. Biol.* **2022**, *6*. Available online: https://7universum.com/ru/nature/archive/item/13855 (accessed on 31 July 2024). (In Russian)
11. Zilitinkevich, S.S. *Fuzzy Logic Controller Based Wind Energy Conversion System*; Fizmatlit: Moscow, Russia, 2013; Volume 252.
12. Beresnev, S.A.; Gryazin, V.I. *Physics of Atmospheric Aerosols: Lecture Course*; Publishing House of Ural University: Yekaterinburg, Russia, 2013; Volume 228. (In Russian)
13. Hewitt, S.; Margetts, L.; Revell, A. Building a digital wind farm. *Arch. Comput. Methods Eng.* **2018**, *25*, 879–899. [CrossRef]
14. VerHulst, C.; Meneveau, C. Large eddy simulation study of the kinetic energy entrainment by energetic turbulent flow structures in large wind farms. *Phys. Fluids* **2014**, *26*, 025113. [CrossRef]
15. Kraposhin, M.V.; Strizhak, S.V. The problem-oriented library SOWFA for solving the applied tasks of wind energy. *Proc. Inst. Syst. Program. RAS (Proc. ISP RAS)* **2018**, *30*, 259–274. [CrossRef]
16. Mehta, D.; Zuijlen, A.H.; Koren, B.; Holierhoek, J.G.; Bijl, H. Large Eddy Simulation of wind farm aerodynamics: A review. *J. Wind Eng. Ind. Aerodyn.* **2014**, *133*, 1–17. [CrossRef]

17. Keck, R.E.; de Maré, M.; Churchfield, M.J.; Lee, S.; Larsen, G.; Madsen, H.A. On Atmospheric Stability in the Dynamic Wake Meandering Model. *Wind Energy* **2014**, *17*, 1689–1710. [CrossRef]
18. Lykosov, V.N. Modeling of processes of interaction of the atmospheric boundary layer with a heterogeneous underlying surface. In Proceedings of the School of Young Scientists and World Conference on Computing and Information Technologies for Environmental Science: "CITES-2017", Tarusa, Zvenigorod, Russia, 28 August–7 September 2017. Available online: http://www.scert.ru/ru/conference/cites2017/ (accessed on 31 July 2024). (In Russian)
19. Hansen, M. *Aerodynamics of Wind Turbines*; Routledge: Abingdon, UK, 2015.
20. Zilitinkevich, S.S.; Laichtman, D.L. On the closure of the system of effective turbulent motion for the atmospheric boundary layer. In *Main Geophysical Observatory Named after A.I. Voeikov. Proceedings: Physics of the Atmospheric Boundary Layer*; Hydrometeorological Publishing House: Leningrad, Russia, 1965; pp. 44–48.
21. Alinot, C.; Masson, C. K-ε model for the atmospheric boundary layer under various thermal stratifications. *J. Sol. Energy Eng.* **2005**, *127*, 438–443. [CrossRef]
22. Alinot, C.; Masson, C. Aerodynamic simulations of wind turbines operating in atmospheric boundary layer with various thermal stratifications. In Proceedings of the ASME 2002 Wind Energy Symposium, Reno, NV, USA, 14–17 January 2002; pp. 206–215. [CrossRef]
23. Kuptsov, A.I.; Akberov, R.R.; Islamkhuzin, D.Y.; Gimranov, F.M. Numerical modeling of the atmospheric boundary layer taking into account its stratification. *Fundam. Res.* **2014**, *9*, 1452–1460. Available online: https://fundamental-research.ru/ru/article/view?id=35083 (accessed on 31 July 2024). (In Russian)
24. Wu, Y.T.; Porté-Agel, F. Large-Eddy Simulati on of Wind-Turbine Wakes: Evaluation of Turbine Parametrisations. *Bound.-Layer Meteorol.* **2011**, *138*, 345–366. [CrossRef]
25. Calaf, M.; Meneveau, C.; Meyers, J. Large eddy simulation study of fully developed wind-turbine array boundary layers. *Phys. Fluids* **2010**, *22*, 015110. [CrossRef]
26. AJha, P.K.; Churchfield, M.J.; Moriarty, P.J.; Schmitz, S. Guidelines for Volume Force Distributions Within Actuator Line Modeling of Wind Turbines on Large-Eddy Simulation-Type Grids. *J. Sol. Energy Eng.* **2014**, *136*, 031003. [CrossRef]
27. Martnez-Tossas, L.A.; Churchfield, M.J.; Leonardi, S. Large eddy simulations of the flow past wind turbines: Actuator line and disk modeling. *Wind Energy* **2014**, *18*, 1047–1060. [CrossRef]
28. Bastankhah, M.; Porte-Agel, F. Wind farm power optimization via yaw angle control: A wind tunnel study. *J. Renew. Sustain. Energy* **2019**, *11*, 023301. [CrossRef]
29. Vermeer, L.J.; Sørensen, J.N.; Crespo, A. VWind turbine wake aerodynamics. *Prog. Aerosp. Sci.* **2003**, *39*, 467–510. [CrossRef]
30. Okulov, V.L. The role of laboratory testing in the development of rotor aerodynamics (review). *Thermophys. Aeromech.* **2018**, *25*, 1–20. [CrossRef]
31. Naumov, I.V.; Mikkelsen, R.F.; Okulov, V.L.; Sørensen, J.N. PIV and LDA measurements of the wake behind awind turbine model. *J. Phys. Conf. Ser.* **2014**, *524*, 012168. [CrossRef]
32. Naumov, I.V.; Mikkelsen, R.F.; Okulov, V.L. Estimation of wake propagation behind the rotors of wind-powered generators. *Therm. Eng.* **2016**, *63*, 208–213.
33. Strijhak, S.V. Mathematical modeling of flow parameters for single wind turbine. *Civ. Aviat. High Technol.* **2016**, *19*, 176–184.
34. Pawar, S.; Sharma, A.; Vijayakumar, G.; Bay, C.J.; Yellapantula, S.; San, O. Towards multi-fidelity deep learning of wind turbine wakes. *Renew. Energy* **2022**, *200*, 867–879. [CrossRef]
35. Calaf, M.; Meneveau, C.; Parlange, M. Large Eddy Simulation study of a fully developed thermal wind-turbine array boundary layer. In *Direct and Large-Eddy Simulation VIII*; Springer: Dordrecht, The Netherlands, 2011; Volume 15, pp. 239–244. [CrossRef]
36. Rasheed, A.; Sorli, K.; Holdahl, R.; Kvamsdal, T.A. Multiscale Approach to Micrositing of Wind Turbines. *Energy Procedia* **2012**, *14*, 1939–1944. [CrossRef]
37. Porté-Agel, F.; Wu, Y.T.; Lu, H.; Conzemius, R.J. Large-eddy simulation of atmospheric boundary layer flow through wind turbines and wind farms. *J. Wind Eng. Ind. Aerodyn.* **2011**, *99*, 154–168. [CrossRef]
38. Kozin, A.A.; Kirpichnikova, I.M. Analysis of a group of vertical-axis wind turbines in the MATLAB software package. *Altern. Energy Ecol.* **2014**, *5*, 45–49.
39. Chock, G.Y.K.; Cochran, L. Modeling of topographic wind speed effects in Hawaii. *J. Wind Eng. Ind. Aerodyn.* **2008**, *93*, 623–638. [CrossRef]
40. O'Sullivan, J.P.; Pecnik, R.; Iaccarino, G. Investigating turbulence in wind flow over complex terrain. In *Proceedings of the Summer Program 2010*; CTR, Stanford University: Stanford, CA, USA, 2010; pp. 129–139.
41. Blocken, B. 50 years of Computational Wind Engineering: Past, present and future. *J. Wind Eng. Ind. Aerodyn.* **2014**, *129*, 69–102. [CrossRef]
42. Mikkelsen, R.F. Actuator Disc Methods Applied to Wind Turbines. Ph.D. Thesis, Technical University of Denmark, Lyngby, Denmark, 2003.
43. Goit, J.; Meyers, J. Optimal control of energy extraction in wind-farm boundary layers. *J. Fluid Mech.* **2015**, *768*, 5–50. [CrossRef]
44. Revaz, T.; Porté-Agel, F. Large-Eddy Simulation of Wind Turbine Flows: A New Evaluation of Actuator Disk Models. *Energies* **2021**, *14*, 3745. [CrossRef]
45. Kovalnogov, V.N.; Fedorov, R.V.; Chukalin, A.V.; Tsvetova, E.V.; Kornilova, M.I. Modeling and Investigation of the Effect of a Wind Turbine on the Atmospheric Boundary Layer. *Energies* **2022**, *15*, 8196. [CrossRef]

46. Aurélien, G. *Hands-On Machine Learning with Scikit-Learn, Keras, and TensorFlow Concepts, Tools, and Techniques to Build Intelligent Systems*, 2nd ed.; O'Reilly Media, Inc.: Sebastopol, CA, USA, 2019; Volume 856.
47. Deep Learning. Available online: https://www.deeplearningbook.org/ (accessed on 31 July 2024).
48. Sozykin, A.V. Review of methods for training deep neural networks. *Bull. SUSU Ser. Comput. Math. Comput. Sci.* **2017**, *6*, 28–59. (In Russian) [CrossRef]
49. Weather and Climate—Weather Forecasts, Weather News, Climate Data. Available online: http://www.pogodaiklimat.ru/ (accessed on 31 July 2024).
50. Open Street Map. Available online: https://www.openstreetmap.org/#map=15/54.2843/48.5974&layers=Y/ (accessed on 31 July 2024).
51. Kolesnikova, T. Construction and training of a neural network for solving the problem of weather forecasting using the Neuroph Studio program. *Compon. Technol.* **2014**, *7*, 129–132.
52. Open Library PyTorch. Available online: https://pytorch.org/docs/stable/generated/torch.nn.BCELoss.html#torch.nn.BCELoss/ (accessed on 31 July 2024).
53. Lam, R.; Sanchez-Gonzalez, A.; Willson, M.; Wirnsberger, P.; Fortunato, M.; Pritzel, A.; Ravuri, S.; Ewalds, T.; Alet, F.; Eaton-Rosen, Z.; et al. GraphCast: Learning skillful medium-range global weather forecasting. *arXiv* **2022**, arXiv:2212.12794.
54. Star CMM+ Singapore. Available online: https://star-ccm.com (accessed on 31 July 2024).
55. Germano, M.; Piomelli, U.; Moin, P.; Cabot, W.H. A Dynamic Subgrid-Scale Eddy Viscosity Model. *Phys. Fluids* **1991**, *3*, 1760–1765. [CrossRef]
56. Lilly, D.K. A proposed modification of the Germano subgrid-scale closure method. *Phys. Fluids* **1992**, *4*, 633–635. [CrossRef]
57. Stevens, R.J.; Martínez-Tossas, L.A.; Meneveau, C. Comparison of wind farm large eddy simulations using actuator disk and actuator line models with wind tunnel experiments. *Renew. Energy* **2018**, *116*, 470–478. [CrossRef]
58. Chamorro, L.P.; Porte-Agel, F. Effects of thermal stability and incoming boundary-layer flow characteristics on wind-turbine wakes: A wind-tunnel study. *Bound.-Layer Meteorol.* **2010**, *136*, 515–533. [CrossRef]
59. Wind Turbine Models—Technical Characteristics of the Vestas V126-3.45 Wind Turbine. Available online: https://en.wind-turbine-models.com/turbines/1249-vestas-v126-3.45 (accessed on 31 July 2024).
60. Yang, X.; Sotiropoulos, F. On the predictive capabilities of LES-actuator disk model in simulating turbulence past wind turbines and farms. In Proceedings of the 2013 American Control Conference, Washington, DC, USA, 17–19 June 2013; IEEE: Manhattan, NY, USA, 2013; pp. 2878–2883. [CrossRef]
61. Sedov, L.I. *Similarity Methods and Dimensional Analysis in Mechanics*; Nauka: Moscow, Russia, 1977; Volume 440. (In Russian)
62. Kovalnogov, V.N.; Fedorov, R.V.; Chukalin, A.V.; Kornilova, M.I.; Karpukhina, T.V.; Petrov, A.V. Application of Intelligent and Digital Technologies to the Tasks of Wind Energy. *Energies* **2023**, *16*, 481. [CrossRef]
63. *GOST R 54084-2010*; Models of the Atmosphere in the Boundary Layer at Altitudes from 0 to 3000 m for Aerospace Practice. Parameters. Standartinform: Moscow, Russia, 2013; 126p. (In Russian)
64. Burton, T.; Sharpe, D.; Jenkins, N.; Bossanyi, E. *Wind Energy: Handbook*; John Wiley and Sons, Ltd.: Chichester, UK, 2001; 642p. [CrossRef]